Soft Matter

ARTICLE TYPE

Cite this: DOI: 00.0000/xxxxxxxxxx

The C36 Laves phase in diblock polymer melts†

Benjamin R. Magruder and Kevin D. Dorfman*

Received Date
Accepted Date

DOI: 00.0000/xxxxxxxxxx

The C14 and C15 Laves phases form as micelle packing structures in many types of soft matter, but the related C36 phase, which consists of alternating C14-type and C15-type layers, has not been observed in any such system. To understand this absence in the context of diblock polymers, we used self-consistent field theory to relate the morphology and energetics of C36 to other known mesophases. Two case studies were conducted: blends of AB diblock polymers with A homopolymers (where A forms the micelle core), in which C14 and C15 have stability windows, and neat AB diblock melts, in which Laves phases are metastable. Laves phases exhibit nearly identical micelle morphologies and nearly degenerate free energies, with the free energy of C36 being a near-perfect bisector of the C14 and C15 free energies in all cases, revealing an intrinsic symmetry in free energy that is attributed solely to the structural relationship between the phases in which the packing of C36 is intermediate between C14 and C15. Based on this connection between structure and free energy, C36 is thus not expected to form in flexible diblock polymers, since C14 and C15 can always form instead via facile mass transfer.

1 Introduction

Self-assembly of compositionally asymmetric amphiphilic molecules into spherical micelles is a ubiquitous phenomenon in soft matter, observed on length scales that vary by orders of magnitude and among molecules with a diverse set of architectures and chemistries.[1,2] At sufficiently high micelle concentration and sufficiently low temperature, micelles self-assemble onto regular 3-dimensional lattices that mimic atomic packings in metals, directly connecting the study of micelles to the study of optimized sphere-packing.[3–5] While it is common to observe simple micellar sphere packing structures with small unit cells, such as body-centered cubic (bcc) or face-centered cubic (fcc) lattices,[6–10] micellar crystals can also form structures with remarkably large and complex unit cells known as Frank-Kasper phases.[11–19] These phases, defined by the framework laid out by Frank and Kasper over 60 years ago,[20,21] are common in metal alloys: 27 Frank-Kasper phases have been observed in metals, with many more theoretically possible.[22] In soft matter, however, only the σ,[23] A15,[24] Z,[19] C14,[25] and C15[26] phases have been observed. Thus, an important open question is whether other Frank-Kasper phases can be formed in soft matter and, if so, what conditions favor their formation.

Laves phases, a subset of Frank-Kasper phases consisting of particles with only 12-fold and 16-fold coordination, are the largest group of intermetallic phases,[27] and have been observed in several types of soft matter.[25,26,28–39] Owing to the volume asymmetry between different particle positions in their lattices, Laves phases tend to form in AB_2 stoichiometries where A is larger than B, exemplified by three Mg alloys, $MgZn_2$, $MgCu_2$, and $MgNi_2$, which form the C14, C15, and C36 Laves phase polytypes, respectively. While many other possible polytypes exist, and some have been found in metal alloys on certain rare occasions, these three are the simplest and are by far the most common.[27] The atomic radius ratio that maximizes space filling in Laves phase metal alloys is $r_A/r_B = \sqrt{1.5}$, resulting in a substantially wider ideal particle size distribution than the σ and A15 phases,[27] the two Frank-Kasper phases that appear most often in soft matter.[3] Laves phases have had a significant presence in recent soft matter literature: C15 was first identified in lipid-based lyotropic liquid crystals in the 1990s,[26,28] while C14 was not observed in similar systems until 2018;[29] C14 and C15 were produced as metastable structures in neat diblock polymer melts,[25,30] and can be stabilized in block polymer systems by blending;[31–37] C14 and C15 were produced via binary blending of giant shape-filling amphiphiles;[38] and finally, C14 was found in a colloidal nanoparticle superlattice.[39]

Amid all of the recent studies on Laves phase formation in soft matter, the C36 Laves phase is conspicuously absent from both experimental results and computational analyses. The purpose of this work is to identify where C36 fits into our understanding of micelle packing structures in soft matter, and flexible diblock polymers in particular. We choose to focus on diblock polymer systems as a model of soft matter because they provide the

Department of Chemical Engineering and Materials Science, University of Minnesota, 421 Washington Ave SE, Minneapolis, MN 55455, USA. E-mail: dorfman@umn.edu

† Electronic Supplementary Information (ESI) available. See DOI: 00.0000/00000000.

most accessible entry point into the investigation of a new candidate mesophase, especially from a computational standpoint. First, as a result of the high degrees of polymerization of the molecules, polymer thermodynamics possesses a degree of universality that can not be applied to smaller molecules like surfactants. Rather than framing self-assembly in the context of local effects like short range van der Waals forces and stereochemistry, polymer behavior can be almost entirely understood by coarsening local-scale phenomena into the Flory-Huggins interaction parameter and through generalized descriptors of polymer architecture, namely the volume-referenced degree of polymerization and statistical segment length.[40] Second, the length scales on which polymer systems self-assemble are such that micelle size and other similar characteristics can be treated as continuous rather than discrete; micelles often consist of hundreds of polymer molecules,[14] and these polymers have radii of gyration that vary in order to fill space at constant density.[41] This nearly continuous degree of reconfigurability in polymer systems is ideally suited for drawing direct connections between lattice structure and thermodynamics, because the system has the flexibility to self-assemble into the most energetically ideal configuration without any significant limitations. While highly discretized micelles, such as those formed by giant shape-filling amphiphiles, may be able to form mesophases that are otherwise unlikely in the absence of discretization,[19,42] a focus on diblock polymers effectively removes these effects and permits a more detailed understanding of the direct structural drivers of mesophase stabilization. Third, sophisticated and accurate computational techniques have been developed to simulate flexible block polymer systems, particularly self-consistent field theory (SCFT), a mean field theory that has proven to be remarkably accurate at predicting order-order transitions between different block polymer mesophases.[43] And fourth, as mentioned above, Laves phases in diblock polymers have received a substantial amount of recent research interest, forming a strong foundation for further research in this space.[25,26,28–39] Thus, our focus herein will be on the use of SCFT to understand the C36 Laves phase in diblock polymer systems.

2 Structure of Laves Phases

The lattice structure onto which micelles are organized affects many characteristics of the corresponding mesophase, including micelle size distribution, average micelle sphericity, and local concentrations of components in a blend, all of which influence the overall free energy.[31,44] Our results will be intimately connected to the structural details of Laves phase packings, and as such it is useful to begin here with an overview of the structures of Frank-Kasper phases, with particular focus on how Laves phases differ from one another.

Frank-Kasper phases are tetrahedrally close-packed, composed of particles of varying size and coordination number (CN), where the CN of a particle is the number of faces on its Wigner-Seitz cell (CN = 12 for fcc, 14 for bcc). Each Wyckoff position (symmetry-equivalent particle position) in the unit cell has a distinct Wigner-Seitz cell, and Frank-Kasper phases consist of multiple Wyckoff positions with CN values of 12, 14, 15, or 16. This results in nonuniformity in Wigner-Seitz cell volumes and sphericities across different particle positions in the unit cell.[44] So, if Frank-Kasper phases form in block polymers, micelles must reconfigure via addition or expulsion of molecules in order to form a different micelle size distribution than was present in either the disordered micelle regime or other ordered mesophases.[35] The thermodynamically preferred mesophase is determined through a subtle balance between enthalpic interactions (e.g. interfacial energies) and packing frustration resulting from the requirement that space be filled at constant density.[41] An important feature of Frank-Kasper phases in soft matter is that the Wigner-Seitz cells have higher average sphericity than fcc or bcc, meaning that densely packed micelles like those in neat diblock polymer melts will have a smaller interfacial area if the Wigner-Seitz cell is imprinted onto the A/B interface, which can be a driving force for stabilization.[44–46]

Laves phases are a subset of Frank-Kasper phases in which all particles are either CN = 12 (smaller particles) or 16 (larger particles). The unit cells of the C14, C15, and C36 Laves phases are shown in Fig. 1a-c for an AB_2 stoichiometry.[27,47,48] However, it is difficult to see the similarities between the three phases when looking only at these unit cells. The similarities are most easily understood using the same layer-stacking description originally employed by Frank and Kasper.[20,21] Each Laves phase consists of a repeated pattern of stacked layers of two distinct types, denoted as Δ and ∇, where the two layer types differ only by a 180° rotation in the plane of the layer. The triangle notation[21] is used in reference to the top-down view of a single layer, in which it appears that a B particle resides at the center of a triangle of other B particles, where the triangle is oriented in the Δ position for a Δ layer and vice versa (shown in Fig. S1[†] and explained further below). C14 consists of alternating Δ and ∇ layers, C15 consists only of layers of the same type (i.e. all Δ or all ∇), and C36 consists of a repeated $\Delta\Delta\nabla\nabla$ pattern. This layer-stacking framework also defines other less common Laves phases, which have longer, more complicated stacking patterns of the two layer types.

If we set the thickness of a single layer equal to one unit in the Cartesian z-direction, with the layer parallel to the x-y plane, we can describe the layers as follows: there is a planar kagomé net of B particles at z = 0, above which a planar triangulated layer of A particles, another of B particles, and a third of A particles are stacked at z = 3/8, 1/2, and 5/8, respectively. A Δ layer can be changed into a ∇ layer by simply swapping the x,y-coordinates of the triangulated layers at z = 1/2 and 5/8. The top-down views of the two layer types (looking down the z-axis of this image or, equivalently, along the [0001] vector of the C14 or C36 unit cell) are shown in Fig. S1.[†] The kagomé net at z = 1, which starts the next layer, is shifted in the x-y plane relative to the kagomé net at z = 0, and the direction of the shift changes sign depends on which layer type lies beneath it. The layer stackings, as well as the shift in the x-y plane between subsequent layers, are clearly visible when the bulk structures of the phases are viewed down the [110] lattice vector ([11$\bar{2}$0] in hexagonal notation), as shown in Fig. 1d-f, where the planes containing a kagomé net are indicated by the dashed lines.

The kagomé net shift in the x-y plane that exists between adja-

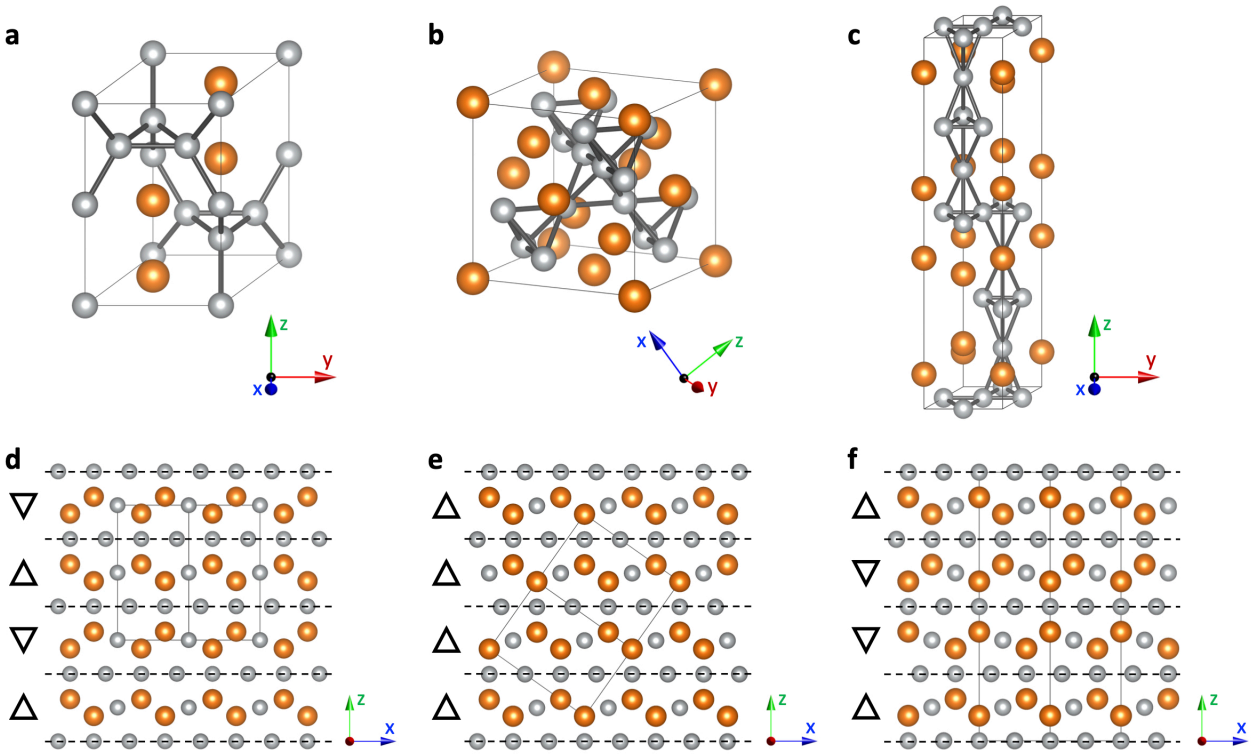

Fig. 1 Unit cell structures of Laves phases (a) C14, (b) C15, and (c) C36 with AB_2 stoichiometry, where A sites are shown as orange spheres and B as gray spheres; lines are drawn between nearest-neighbor B sites as visual aids. View of bulk lattice down the [110] vector ([11$\bar{2}$0] in hexagonal notation) for (d) C14, (e) C15, and (f) C36, showing four stacked layers with horizontal dashed lines indicating the start of each layer, and Δ or ∇ labels for each layer. Cartesian x, y, and z directions are defined such that z is perpendicular to the Laves phase layers, and y is parallel to an arbitrarily chosen line in the kagomé net. Solid gray lines in the background indicate the boundary of a single unit cell. Figure generated using VESTA.[47]

cent layers allows for an additional method through which the Laves phase layer stackings can be categorized, known as the Jagodzinski-Wyckoff notation.[49] In this notation, a layer is categorized based on the direction of the shift of the layers directly above and below it. If both such layers are displaced in the same direction (i.e. if the kagomé nets immediately above and below the layer are identical in the x-y plane), then the middle layer is denoted by the letter h. If the opposite is true and the layers above and below are shifted in opposite directions, the middle layer is denoted by the letter c. Thus, all C14 layers are h layers, all C15 layers are c layers, and C36 layers alternate repeatedly between c and h, which can be seen clearly in Fig. 1d-f. In this way, C36 can be thought of as being structurally intermediate between C14 and C15, with half of its layers being C14-like and half being C15-like. This construction will prove to be a key geometric element underlying our results.

3 Self-Consistent Field Theory

In this paper, we present SCFT calculations for neat diblock polymer melts and diblock/homopolymer blends in the canonical ensemble. Our implementation of SCFT uses the Gaussian chain model to represent the behavior of flexible polymers. SCFT is strictly valid in the mean-field limit (in which the invariant degree of polymerization goes to infinity) and is known to be inaccurate primarily when studying conditions that are near the order-disorder transition.[43] The remainder of this section will consist of a brief overview of the SCFT equations as they pertain to the polymer melts and blends considered in this work,[43,50–52] as well as the details of their implementation.

First, we will introduce the notation that will be used to describe our polymer systems. In AB diblock polymers, A will refer to the minority block. The degree of segregation between repeat units of A and B is represented by χN, where χ is the Flory-Huggins interaction parameter between monomer types A and B, and N is the degree of polymerization of the diblock polymer. An important factor driving the stabilization of Frank-Kasper phase micelle packings is the degree of conformational asymmetry,[16,53] quantified as the ratio of statistical segment lengths, $\varepsilon = b_A/b_B$, where b is the statistical segment length of a single repeat unit.[54,55] The compositional asymmetry of an AB diblock polymer is represented by f_A, the volume fraction of block A in a neat AB melt. In blends of AB diblock polymers with A homopolymers of degree of polymerization N_H, the overall volume fraction of diblock polymer in the composite system will be denoted by ϕ_D. When discussing blends, χN is reported using the N value of the diblock polymer. The other important parameter in these blends is the ratio of homopolymer length to A block length, which we denote as $\alpha = N_H/N_A$ (where N_A refers to the length of the A block in the diblock polymer).

Using this notation, we introduce the SCFT equations for the specific case of blends of AB diblock polymers and A homopolymers, which can be applied to neat AB diblock polymer melts by

setting $\phi_D = 1$. We consider a system in a unit cell of volume V containing 2 monomer types, labeled as α = A or B, each of which has a chemical potential and volume fraction at every position $\mathbf{r}$, denoted as $\omega_\alpha(\mathbf{r})$ and $\phi_\alpha(\mathbf{r})$, respectively. The contour of the block polymer runs from $s \in [0, N_D]$ and the corresponding range for the homopolymer is $s \in [0, N_H]$. The objective of SCFT is to find a self-consistent solution to the chemical potential field for each species using the pair of equations

$$\begin{aligned} \omega_A(\mathbf{r}) &= \chi\phi_B(\mathbf{r}) + \xi(\mathbf{r}) \\ \omega_B(\mathbf{r}) &= \chi\phi_A(\mathbf{r}) + \xi(\mathbf{r}), \end{aligned} \tag{1}$$

where $\xi(\mathbf{r})$ is a Lagrange multiplier pressure field, subject to the incompressibility constraint

$$\phi_A(\mathbf{r}) + \phi_B(\mathbf{r}) = 1. \tag{2}$$

The volume fractions are computed from

$$\begin{aligned} \phi_A(\mathbf{r}) = &\frac{\phi_D}{N_D Q_D} \int\limits_{\alpha(s)=A} \mathrm{d}s\, q_D(\mathbf{r},s) q_D^\dagger(\mathbf{r},s) \\ &+ \frac{1-\phi_D}{N_H Q_H} \int \mathrm{d}s\, q_H(\mathbf{r},s) q_H(\mathbf{r}, N_H - s) \end{aligned} \tag{3}$$

and

$$\phi_B(\mathbf{r}) = \frac{\phi_D}{N_D Q_D} \int\limits_{\alpha(s)=B} \mathrm{d}s\, q_D(\mathbf{r},s) q_D^\dagger(\mathbf{r},s), \tag{4}$$

where $\alpha(s)$ refers to whatever monomer type is located at position s along the chain. Q_i is the normalized overall partition function for each species i, defined by the equation

$$Q_i = \frac{1}{V} \int \mathrm{d}\mathbf{r}\, q_i(\mathbf{r}, s = N_i). \tag{5}$$

The propagators $q_i(\mathbf{r},s)$ and $q_i^\dagger(\mathbf{r},s)$ satisfy the modified diffusion equations

$$\begin{aligned} \frac{\partial q_i(\mathbf{r},s)}{\partial s} &= \left[\frac{b_{\alpha(s)}^2}{6} \nabla^2 - \omega_{\alpha(s)}(\mathbf{r}) \right] q_i(\mathbf{r},s) \\ -\frac{\partial q_i^\dagger(\mathbf{r},s)}{\partial s} &= \left[\frac{b_{\alpha(s)}^2}{6} \nabla^2 - \omega_{\alpha(s)}(\mathbf{r}) \right] q_i^\dagger(\mathbf{r},s). \end{aligned} \tag{6}$$

The initial conditions used in solving the above equations are $q_i(\mathbf{r},0) = q_i^\dagger(\mathbf{r},N_i) = 1$.

In SCFT, the fields ω_A and ω_B are adjusted to achieve a self-consistent solution, whereupon the mean-field Helmholtz free energy F per monomer is calculated as

$$\begin{aligned} \frac{F}{k_B T} \frac{v}{V} = &\frac{\phi_D}{N_D} \left[\ln\left(\frac{\phi_D}{Q_D}\right) - 1 \right] + \frac{\phi_H}{N_H} \left[\ln\left(\frac{\phi_H}{Q_H}\right) - 1 \right] \\ &- \frac{1}{V} \int \mathrm{d}\mathbf{r}\, \left[\omega_A(\mathbf{r})\phi_A(\mathbf{r}) + \omega_B(\mathbf{r})\phi_B(\mathbf{r}) + \chi\phi_A(\mathbf{r})\phi_B(\mathbf{r}) \right], \end{aligned} \tag{7}$$

where $k_B T$ is the thermal energy and v is the average volume per repeat unit, or the "reference volume." Since the Flory-Huggins theory giving rise to χ is predicated on a lattice model using that reference volume, it is necessary to define all repeat units such that they have volume v, so the degree of polymerization of all blocks and the statistical segment length of all monomer types are normalized to the same reference volume. All calculations presented in this work use volume-referenced degrees of polymerization and statistical segment lengths.

The open-source Polymer Self-Consistent Field software package (PSCF) was used to perform all calculations herein, and the reader is directed to the original references for PSCF for further information.[52,56] The Anderson Mixing iterative algorithm used to solve the above equations while simultaneously optimizing the unit cell parameters is described in detail elsewhere, including information about tolerance and convergence criteria,[56–58] and several other works have provided a physical interpretation and derivation of the above equations.[43,50–52]

All calculations were performed with a tolerance in the self-consistent field equations of 10^{-5} and an integration step size of 0.01. All free energies are reported on a per chain basis. The grid sizes used for each mesophase are (discretizing the primitive unit cell for each structure): A15 = $64 \times 64 \times 64$; bcc = $48 \times 48 \times 48$; fcc = $36 \times 36 \times 36$; hex = 64×64; σ = $128 \times 128 \times 64$; Z = $64 \times 64 \times 64$; C14 = $64 \times 64 \times 104$; C15 = $96 \times 96 \times 96$; C36 = $64 \times 64 \times 210$. The high resolution Laves phase calculations were performed using an integration step size of 0.005 and grid sizes as follows: C14 = $96 \times 96 \times 156$; C15 = $124 \times 124 \times 124$; C36 = $80 \times 80 \times 263$. In these cases, the convergence tolerance was also reduced to 10^{-6} for C14.

Some results presented here were calculated in a similar form in previous publications.[25,32] Those data were recalculated for this paper to ensure consistency, with the exception of the fcc, hex, and σ data in Fig. S4,[†] which were computed and originally published by Kim et al.[25] Otherwise, converged solutions from previous published work were used as initial guesses, where applicable.

4 Results

We have considered how C36 fits into the existing understanding of Laves phase formation in diblock polymers that has rapidly developed over the past several years.[25,30–36] The two pertinent case studies used to accomplish this are neat melts of AB diblock polymers, following the work of Kim et al.,[25] and blends of AB with A homopolymer, following several recent studies[31–33] (hereafter referred to as AB melts and AB/A blends, respectively). In the former, Laves phases are not observed to be the thermodynamically preferred micelle packing structure.[25] This is perhaps unsurprising, because the difference between the largest and smallest Wigner-Seitz cell is much larger in Laves phases than in the more frequently observed σ and A15 Frank-Kasper phases, meaning that Laves phases require a greater degree of chain stretching and packing frustration to form in monodisperse neat melts. However, blending with A homopolymer introduces additional degrees of freedom that permit greater particle size asymmetry without introducing a substantial chain stretching penalty, opening up a Laves phase stability window throughout which C14 and C15 are nearly degenerate.[32,33] Laves phases are only stable in these AB/A blends when the homopolymer length is at least

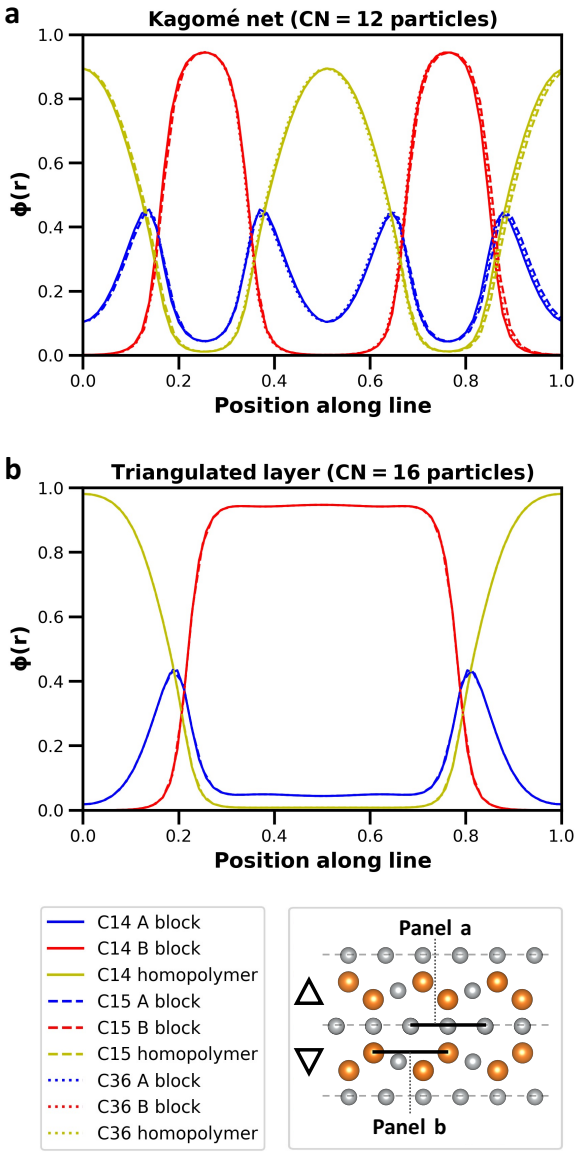

Fig. 2 Local volume fraction $\phi(\mathbf{r})$ of each species in an AB/A blend, plotted as a function of position along a line within the unit cell of each Laves phase. The locations of the lines are (a) through three collinear particles within a single kagomé net of smaller (CN = 12) particles, and (b) through two adjacent particles in a triangulated layer of the larger (CN = 16) particles, as visualized in the layer side-view shown at the bottom-right corner of the figure. Note that the particles shown in this layer side-view are not coplanar; they have different heights in the direction perpendicular to the page. Data were calculated using SCFT at $\chi N = 25$, $\varepsilon = b_A/b_B = 1.31$, and $f_A = 0.18$. The volume fraction of the A block is shown in blue, the B block is shown in red, and the A homopolymer is shown in yellow; data for the C14 mesophase are shown as a solid line, C15 is shown as a dashed line, and C36 is shown as a dotted line. Data are shown for the dry-brush regime ($\alpha = 1$, where $\alpha = N_H/N_A$) at bulk diblock polymer volume fraction $\phi_D = 0.85$, a condition for which C15 is the preferred mesophase.

roughly the same as that of the A block of the diblock, in which case the homopolymer tends to segregate to the center of the micelle core, leaving the A block closer to the A/B interface. This is referred to as the "dry-brush regime." When the homopolymer length is significantly shorter than the A block, in the "wet-brush regime," the segregation does not occur to nearly the same degree, and the Laves phases do not have a window of stability. A breakdown of the different contributions to the free energy reveals that, in the dry brush regime, the Laves phases are stabilized due to substantially lower interaction free energy between the B block and the homopolymer compared to other mesophases;[31–33] additionally, an observed transition from C14 to C15 upon adding more homopolymer is driven by a slight difference between the two mesophases in interaction free energy between the A and B blocks.[33]

We begin by incorporating C36 into prior computational results for AB/A blends. In order to simplify calculations and maintain comparability with previous studies, we fix $\chi N = 25$, $f_A = 0.18$, and conformational asymmetry $\varepsilon = 1.31$, emulating the experiments of Mueller et al.[31] on poly(styrene-*block*-1,4-butadiene) and the subsequent SCFT studies.[32,33] The two parameters of interest are α and ϕ_D. Here, we use $\alpha = 1$ for dry-brush regime calculations and $\alpha = 7/9$ for the wet-brush regime; these values of α have been previously shown using SCFT to possess the qualitative characteristics of their respective regimes in accordance with experiments.[31,32] The relevant range of ϕ_D spans from 0.75 to 1, because mesophase diagrams at lower values of of ϕ_D primarily consist of a large two-phase window.[33]

First, we determine whether the SCFT results reveal differences in the morphologies of the self-assembled micelles between the C14, C15, and C36 mesophases. From SCFT, the 3-dimensional concentration profiles for each species are accessible, and can be directly compared across mesophases. These concentration profiles are expected to vary depending on whether the system is in the wet-brush or dry-brush regime, on the bulk volume fraction of the homopolymer, and on the Wyckoff position of the particle(s) under consideration (and, by proxy, the Wigner-Seitz cell volume and CN of the particle). The complete SCFT solution takes the form of a unit cell that looks like Figs. 1a-c, and directly comparing these unit cells can be visually difficult, so it is most effective to lower the dimensionality of the data by observing a 1D line profile or a 2D contour plot when comparing the SCFT solutions of different mesophases.

Figure 2 shows two such line profiles for the case of $\alpha = 1$, $\phi_D = 0.85$, a condition for which C15 is the preferred mesophase. The first, Fig. 2a, traces a path through three collinear small (CN = 12) particles within a single kagomé net; the local volume fraction of A block, B block, and A homopolymer in each of the three Laves phases is plotted as a function of position along this line. It was found that choosing a different set of three particles within the same unit cell does not affect the resulting trend, so they are chosen arbitrarily here and the result can be considered general to any particles within the kagomé net. The second line profile, Fig. 2b, represents species concentrations along a line connecting two adjacent large particles (CN = 16) within the same triangulated layer (i.e. both particles at z = 3/8 or both at z = 5/8 in our above description of the Δ and ∇ layers). A side view of two stacked Laves phase layers is shown at the bottom of the figure to demonstrate visually some examples of where the line profiles are located within a layer.

The results of Fig. 2 imply that the concentration profiles

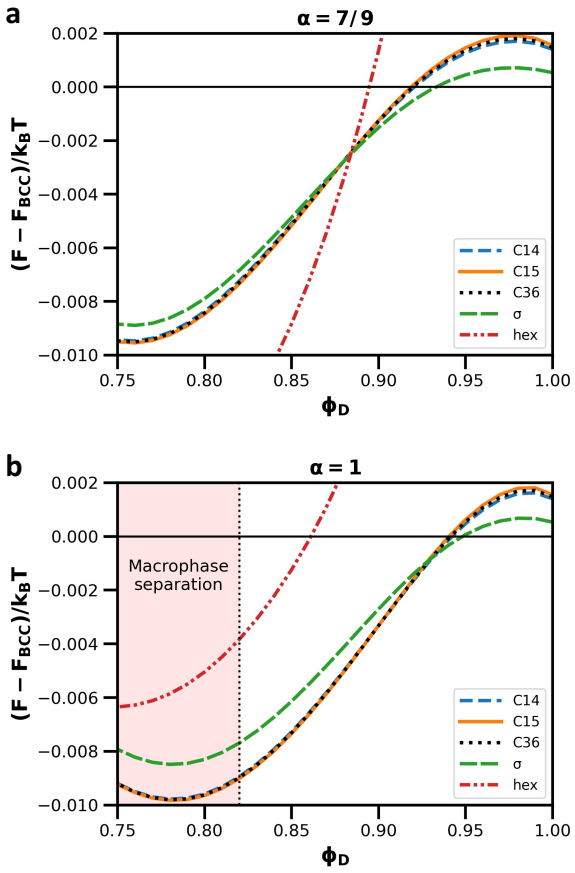

Fig. 3 Helmholtz free energy per chain in an AB/A blend relative to the free energy of the bcc mesophase, calculated using SCFT at $\chi N = 25$, $f_A = 0.18$, and $\varepsilon = b_A/b_B = 1.31$ as a function of AB diblock polymer volume fraction ϕ_D. Data are shown for (a) the wet-brush regime ($\alpha = 7/9$, where $\alpha = N_H/N_A$) and (b) the dry-brush regime ($\alpha = 1$).

within a single layer are nearly identical across the three Laves phases. There are some small regions in Fig. 2a where the Laves phases do not exactly overlap with one another, which can be attributed to the fact that the distribution of Wigner-Seitz cell volumes for the smaller CN = 12 particles varies slightly between Laves phases,[5,34] and the micelle size distribution is expected to demonstrate similar variation. No such variation is evident in Fig. 2b, in which all three Laves phases overlap such that the dashed and dotted lines are indistinguishable from the solid lines; this is in agreement with the pattern observed in the Wigner-Seitz cells of the larger CN = 16 particles, which all have identical volumes in each Laves phase.

Line profiles were also calculated for the wet-brush regime ($\alpha = 7/9$), and at a higher diblock volume fraction $\phi_D = 0.92$, at which composition C14 is the preferred mesophase in the dry-brush regime. The results are presented in Figs. S2 and S3†, showing trends that are effectively the same as those seen in Fig. 2. It is also worth noting that increased homopolymer localization at the center of the micelle core in the dry-brush regime is visually evident in these figures. Furthermore, 2D contour plots are presented in Fig. S4†, giving a qualitative visualization of the shape of the micelle cores. It is evident from these contour plots that the smaller CN = 12 particles are substantially nonspherical, as expected based on the Wigner-Seitz cell geometries,[34] and that the cores of the larger CN = 16 sites are almost perfectly spherical. The shapes of the micelle cores for both small and large particles appear qualitatively identical across the three Laves phases in these contour plots, further emphasizing the similarity in micelle morphology.

Additionally, SCFT calculations optimize the unit cell parameters to minimize free energy, and it was determined that all Laves phases have functionally identical unit cell volumes per particle under all conditions tested, shown in Fig. S5† for both AB melts and AB/A blends. Seeing no evidence to the contrary in either the lattice structures themselves or in the data of Fig. 2 and Figs. S2-S5†, we conclude that the three mesophases form an approximately identical set of micelles with regards to size, shape, and homopolymer distribution.

While our focus herein is on equilibrium configurations, the morphological similarity between Laves phase micelles does have implications regarding the kinetics of mesophase transitions that are worth noting briefly. The nearly identical micelle size distribution across Laves phases means that transitioning from one Laves phase to another does not require substantial chain exchange between micelles. The slight differences in micelle sizes that are evident in Fig. 2a may lead to a small number of chains moving between micelles during a transition between Laves phases, but the chain exchange will be negligible relative to that which would be required to transition to a non-Laves phase. This significantly lowers the energetic barrier to mesophase transitions compared to transitions that require the energetically unfavorable process of redistributing micelle sizes, a process which has been discussed extensively elsewhere.[35] This implies that, if a Laves phase is formed, it will almost certainly be the most stable of the three rather than a kinetic trapping of a less favored mesophase, because transitioning to the most stable mesophase is expected to be facile.

Although the morphologies of the micelles within each Laves phase are effectively equivalent, their free energies differ due to the arrangement of those micelles. The Helmholtz free energy profile of all mesophases of interest from SCFT are shown in Fig. 3, plotted as a free energy difference between the mesophase of interest and bcc. As is evident from both panels of the figure, the Laves phases are nearly degenerate under all conditions tested, to the point of being virtually indistinguishable from one another on the plot — a detail we will return to shortly. This near-degeneracy is unsurprising based on the the vast similarities between the different Laves phase structures and the micelle morphologies, and is in agreement with previous studies of C14 and C15.[25,32,33] Cheong et al.[32] also used grand-canonical SCFT for this system to determine that macrophase separation between a homopolymer-rich and a homopolymer-poor mesophase will occur at sufficiently high homopolymer concentrations, which is indicated by the shaded region on Fig. 3b. A15, Z, and fcc were also tested as candidate mesophases, but showed no regions of stability with the exception of fcc in a very small window at $\phi_D \approx 1$. Fig. S6† shows how the free energies of these three additional mesophases compare to those shown in Fig. 3.

It is also useful to consider a different polymer system in order

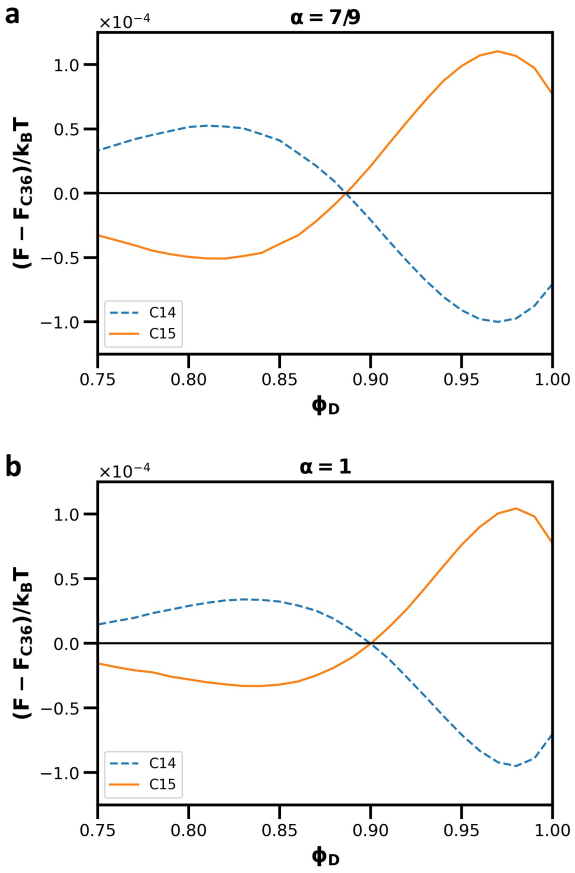

Fig. 4 Helmholtz free energy per chain of Laves phases in an AB/A blend relative to the free energy of the C36 mesophase, calculated using SCFT at $\chi N = 25$, $f_A = 0.18$, and $\varepsilon = b_A/b_B = 1.31$ as a function of AB diblock polymer volume fraction ϕ_D. Data are shown for (a) the wet-brush regime ($\alpha = 7/9$, where $\alpha = N_H/N_A$) and (b) the dry-brush regime ($\alpha = 1$).

to see whether the behavior seen in Fig. 3 is merely a result of the multicomponent nature of the blend. To address this question, free energy profiles were calculated for neat diblock polymer melts as a function of χN, ε, and f_A, shown in Fig. S7,† incorporating C36 into the free energy profiles previously published by Kim et al.[25] As with AB/A blends, Laves phases are nearly degenerate in pure diblock polymer melts under all conditions tested, indicating that the near-degeneracy is characteristic of Laves phases in diblock polymer systems generally rather than a specific result of the blended system.

Upon looking closely at the Laves phase free energy profiles on Fig. 3 and Fig. S7,† it appears that C36 has a free energy that is always intermediate between C14 and C15 in all regions of the figures for which a difference can be distinguished. In order to investigate this further, we used high resolution SCFT to generate free energies with sufficient accuracy to allow for the parsing of the data in greater detail. The results for the AB/A blend, shown in Fig. 4, are presented by plotting the free energy of C14 and C15 relative to the free energy of C36. These more detailed calculations reveal an intrinsic symmetry in the free energy profiles as a function of composition that is not obvious from lower resolution SCFT calculations. The free energy of the C36 mesophase is a near-perfect bisector of the free energies of the C14 and C15 mesophases at all relevant blend compositions.

It is noteworthy, however, that the bisection is not exact to within the expected error of the calculation; this is evident by evaluating the absolute value of the lines from Fig. 4 and replotting, which is shown in Fig. S8.† These additional plots reveal that the absolute values of the lines differ by $1 \times 10^{-5}\,kT$ at most, at the point where the absolute values themselves are the largest. This difference, albeit small, is an important caveat, because even in this idealized and entirely reconfigurable simulated system there are still small phenomena that prevent the lattice symmetry from being reflected perfectly in the thermodynamics.

It is equally worthwhile to perform a similar analysis for a neat AB diblock polymer melt, in order to determine the degree to which this symmetry can be expected to be universal for Laves phases in soft matter. The results, shown in Fig. 5 for several values of χN and ε, reveal the same intrinsic symmetry that was present in the diblock/homopolymer blend. Plots of the absolute values of these lines are also shown in Fig. S8,† revealing that the absolute values differ by $2.2 \times 10^{-5}\,kT$ at most.

5 Discussion

Our results can best be understood in the context of the layer stackings of Laves phases, as alluded to in Section 2. Using the Jagodzinski-Wyckoff notation, C36 is denoted as a stack of layers with exactly half of its layers being C14-type and half being C15-type. The bisection of the C14 and C15 free energies by C36 implies that the free energy of an h layer differs to a small degree from that of a c layer, and that this difference is the only factor contributing to the free energy differences between Laves phases (neglecting the minor differences in Fig. S8†). Or, presented another way, we can consider two adjacent layers to have an effective "interfacial energy" between them, where a $\Delta\nabla$ pair (or $\nabla\Delta$, which is identical) is energetically different from a $\Delta\Delta$ (or $\nabla\nabla$) pair to a small degree. C14 contains only $\Delta\nabla$ pairs, C15 contains only $\Delta\Delta$ pairs, and C36 contains 50% of each. In this way, the "interfacial energy" between layers is the only significant variable distinguishing the free energies of the Laves phases.

As a consequence of this result, we expect that the C36 symmetry cannot form in self-assembled diblock polymer micelle packings, because the symmetry can be easily reconfigured within the melt — without substantially changing the micelle size distribution — to either C14 or C15, one of which should always have a slightly lower free energy than C36. In other soft matter systems on smaller length scales, such as liquid crystals, the question of the potential existence of C36 is less easily resolved due to the consequences of short range effects that may stabilize C36 in the same way that it is stabilized in metal alloys. The energetics of Laves phases may also be different in polymer systems that contain unique geometries, such as branched polymers or multiblock polymers, or that contain semiflexible/rigid polymers that are not described well by the Gaussian chain model, and the results herein for diblock polymers should not necessarily be generalized to such systems without further justification.

It is worthwhile, in the context of the above results, to revisit the analogy between solid state lattices in metallurgy and micelle packing in soft matter systems, which has proven to be a very use-

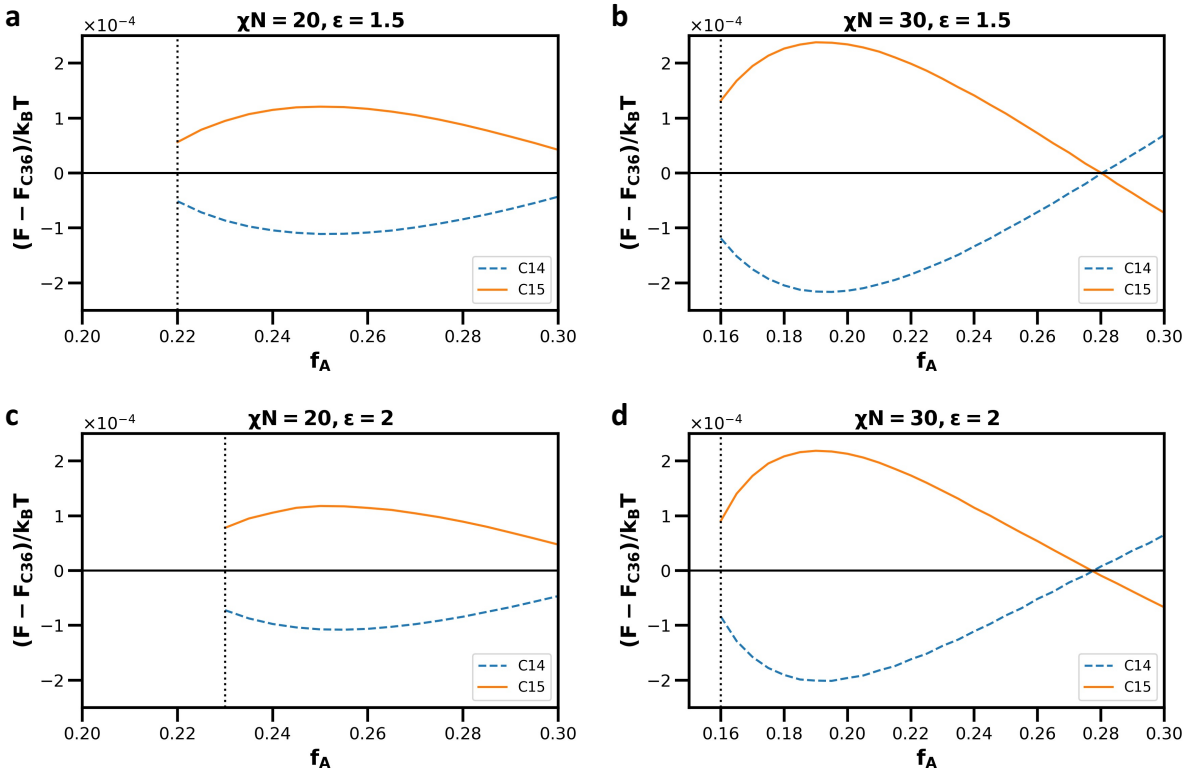

Fig. 5 Helmholtz free energy per chain of Laves phases in neat AB diblock polymer melts relative to the free energy of the C36 mesophase, calculated using SCFT as a function of A block volume fraction f_A. Data are shown at $\chi N = 20, 30$ and $\varepsilon = b_A/b_B = 1.5, 2$.

ful way to understand the results of some recent studies.[25,29,35,44] Metals have a plethora of phenomena that all contribute to the determination of the preferred lattice structure, from defect concentrations and atomic radii to valence electron concentrations and band effects, all of which have a role to play in Laves phase formation.[49,59] The phenomena that affect the preferred Laves phase in a given alloy are generally known, but it is extremely difficult to use this knowledge in any broadly predictive way because all of the effects are intricately entangled with one another.[49,59] Thus, the explanation for why a particular structure will preferentially form in a metal requires far more than just an evaluation of the geometry of the lattice. In this sense, studying the formation of these lattices in soft matter systems — and diblock polymers in particular — allows the effects of the structure itself to be uniquely isolated, stripping away the impact of the chemical details of short-range forces and discrete particle sizes through the universality and reconfigurability of the systems. The results reported here regarding Laves phases in equilibrium diblock polymers represent the most extreme version of this scenario, where the structure is the *only* relevant factor determining the preferred mesophase, causing C36 to be relegated to the position of having only intermediate stability among the three Laves phases under all circumstances. So, the metal/soft matter analogy breaks down to a certain extent here: a phase that is prevalent in metals (C36) appears unlikely to form as a mesophase in diblock polymers, a form of soft matter. Conversely, the breakdown of the analogy also implies that a Frank-Kasper phase may very well be stable in soft matter even if it is not observed in any metal alloy. The lattice structure, then, appears to have a higher degree of importance in diblock polymers than in metal alloys when it comes to predicting the equilibrium phase behavior.

6 Concluding Remarks

In summary, we have shown using SCFT that the C36 Laves phase is not a preferred micelle packing structure in AB and AB/A diblock polymer systems, but rather exists as an energetically intermediate structure between C14 and C15 under all conditions examined. The difference in free energy between the Laves phases results solely from their layer-stacking architectures, where a $\Delta\nabla$ (or $\nabla\Delta$) pair of layers differs in energy from a $\Delta\Delta$ (or $\nabla\nabla$) pair. This is evident from the fact that the free energy of C36, a mesophase with half C14-like and half C15-like layers, always bisects the free energies of the C14 and C15 mesophases. Based on 1D line profiles and 2D contour plots generated from the converged SCFT solutions, the three Laves phases are shown to have functionally equivalent micelle morphologies, meaning that transitions from one Laves phase to another requires negligible chain exchange between micelles. This leads to the conclusion that C36 will not form in diblock polymers because either C14 or C15 will be more stable and can be formed easily from the same micelle morphologies. However, C36 formation may still be possible in other soft matter systems as a result of short-range effects that do not exist in the diblock polymer mesophases studied here. The analogy between micelle packings in soft matter and atomic packings in metals breaks down when considering C36 in diblock polymers, but remains a useful platform to discuss relationships

between mesophases nonetheless. Further work to build upon these results may consider ways in which C36 could be stabilized in other forms of soft matter. Additionally, the fact that lattice structure is connected so directly to free energy in these systems may open up new ways to rationalize why some Frank-Kasper phases form in soft matter and some do not.

Author Contributions

B.R.M. and K.D.D. designed research, analyzed data, prepared manuscript, and edited manuscript; B.R.M. performed research.

Conflicts of interest

There are no conflicts to declare.

Acknowledgements

We acknowledge Guo Kang Cheong, Logan Case, and Akash Arora, whose scripts and SCFT calculations were very useful as tools to help generate the data herein. This work was supported by the NSF Grant DMR-1725272. Computational resources were provided by the Minnesota Supercomputing Institute.

References

1 R. A. L. Jones, *Soft Condensed Matter*, Oxford University Press, Oxford, 2002.

2 Z. Su, M. Huang and S. Z. D. Cheng, *Proc. Natl. Acad. Sci. USA*, 2020, **117**, 19618–19620.

3 M. Huang, K. Yue, J. Wang, C.-H. Hsu, L. Wang and S. Z. D. Cheng, *Sci. China Chem.*, 2018, **61**, 33–45.

4 N. Xie, M. Liu, H. Deng, W. Li, F. Qiu and A.-C. Shi, *J. Am. Chem. Soc.*, 2014, **136**, 2974–2977.

5 A. Reddy, M. B. Buckley, A. Arora, F. S. Bates, K. D. Dorfman and G. M. Grason, *Proc. Natl. Acad. Sci. USA*, 2018, **115**, 10233–10238.

6 L. Leibler, *Macromolecules*, 1980, **13**, 1602–1617.

7 F. S. Bates, R. E. Cohen and C. V. Berney, *Macromolecules*, 1982, **15**, 589–592.

8 A. N. Semonov, *Macromolecules*, 1989, **22**, 2849–2851.

9 P. Sakya, J. M. Seddon, R. H. Templer, R. J. Mirkin and G. J. T. Tiddy, *Langmuir*, 1997, **13**, 3706–3714.

10 D. J. P. Yeardley, G. Ungar, V. Percec, M. N. Holerca and G. Johansson, *J. Am. Chem. Soc.*, 2000, **122**, 1684–1689.

11 C. Tschierske, *Angew. Chem. Int. Ed.*, 2013, **52**, 8828–8878.

12 G. Ungar and X. Zeng, *Soft Matter*, 2005, **1**, 95–106.

13 S. A. Kim, K.-J. Jeong, A. Yethiraj and M. K. Mahanthappa, *Proc. Natl. Acad. Sci. USA*, 2017, **114**, 4072–4077.

14 S. Lee, M. J. Bluemle and F. S. Bates, *Science*, 2010, **330**, 349–353.

15 M. W. Bates, J. Lequieu, S. M. Barbon, R. M. Lewis, K. T. Delaney, A. Anastasaki, C. J. Hawker, G. H. Fredrickson and C. M. Bates, *Proc. Natl. Acad. Sci. USA*, 2019, **116**, 13194–13199.

16 N. Xie, W. Li, F. Qiu and A.-C. Shi, *ACS Macro Lett.*, 2014, **3**, 906–910.

17 M. Watanabe, Y. Asai, J. Suzuki, A. Takano and Y. Matsushita, *Macromolecules*, 2020, **53**, 10217–10224.

18 M. Huang, C.-H. Hsu, J. Wang, S. Mei, X. Dong, Y. Li, M. Li, H. Liu, W. Zhang, T. Aida, W.-B. Zhang, K. Yue and S. Z. D. Cheng, *Science*, 2015, **348**, 424–428.

19 Z. Su, C.-H. Hsu, Z. Gong, X. Feng, J. Huang, R. Zhang, Y. Wang, J. Mao, C. Wesdemiotis, T. Li, S. Seifert, W. Zhang, T. Aida, M. Huang and S. Z. D. Cheng, *Nat. Chem.*, 2019, **11**, 899–905.

20 F. C. Frank and J. S. Kasper, *Acta Crystallogr.*, 1958, **11**, 184–190.

21 F. C. Frank and J. S. Kasper, *Acta Crystallogr.*, 1959, **12**, 483–499.

22 M. D. Sikirić, O. Delgado-Friedrichs and M. Deza, *Acta Crystallogr., Sect. A: Found. Crystallogr.*, 2010, **66**, 602–615.

23 G. Ungar, Y. Liu, X. Zeng, V. Percec and W.-D. Cho, *Science*, 2003, **299**, 1208–1211.

24 R. Vargas, P. Mariani, A. Gulik and V. Luzzati, *J. Mol. Biol.*, 1992, **225**, 137–145.

25 K. Kim, M. W. Schulze, A. Arora, R. M. Lewis, M. A. Hillmyer, K. D. Dorfman and F. S. Bates, *Science*, 2017, **356**, 520–523.

26 J. M. Seddon, *Biochemistry*, 1990, **29**, 7997–8002.

27 F. Stein and A. Leineweber, *J. Mater. Sci.*, 2021, **56**, 5321–5427.

28 V. Luzzati, R. Vargas, A. Gulik, P. Mariani, J. M. Seddon and E. Rivas, *Biochemistry*, 1992, **31**, 279–285.

29 C. M. Baez-Cotto and M. K. Mahanthappa, *ACS Nano*, 2018, **12**, 3226–3234.

30 S. Jeon, T. Jun, S. Jo, H. Ahn, S. Lee, B. Lee and D. Y. Ryu, *Macromol. Rapid Commun.*, 2019, **40**, 1900259.

31 A. J. Mueller, A. P. Lindsay, A. Jayaraman, T. P. Lodge, M. K. Mahanthappa and F. S. Bates, *ACS Macro Lett.*, 2020, **9**, 576–582.

32 G. K. Cheong, F. S. Bates and K. D. Dorfman, *Proc. Natl. Acad. Sci. USA*, 2020, **117**, 16764–16769.

33 J. Xie and A.-C. Shi, *Giant*, 2021, **5**, 100043.

34 M. Zhao and W. Li, *Macromolecules*, 2019, **52**, 1832–1842.

35 K. Kim, A. Arora, R. M. Lewis, M. Liu, W. Li, A.-C. Shi, K. D. Dorfman and F. S. Bates, *Proc. Natl. Acad. Sci. USA*, 2018, **115**, 847–854.

36 S. Xie, A. P. Lindsay, F. S. Bates and T. P. Lodge, *ACS Nano*, 2020, **14**, 13754–13764.

37 M. H. Uddin, C. Rodriguez, A. López-Quintela, D. Leisner, C. Solans, J. Esquena and H. Kunieda, *Macromolecules*, 2003, **36**, 1261–1271.

38 Y. Liu, T. Liu, X.-y. Yan, Q.-Y. Guo, J. Wang, R. Zhang, S. Zhang, Z. Su, J. Huang, G.-X. Liu, W. Zhang, W. Zhang, T. Aida, K. Yue, M. Huang and S. Z. D. Cheng, *Giant*, 2020, **4**, 100031.

39 S. Hajiw, B. Pansu and J.-F. Sadoc, *ACS Nano*, 2015, **9**, 8116–8121.

40 T. P. Lodge and P. C. Hiemenz, *Polymer Chemistry*, CRC Press, Boca Raton, 3rd edn, 2020.

41 A.-C. Shi, *J. Phys. Condens. Matter*, 2021, **33**, 253001.

42 A. Reddy and G. M. Grason, *Nat. Chem.*, 2019, **11**, 865–867.

43 G. H. Fredrickson, *The Equilibrium Theory of Inhomogeneous*

Polymers, Oxford University Press, Oxford, 2006.
44 S. Lee, C. Leighton and F. S. Bates, *Proc. Natl. Acad. Sci. USA*, 2014, **111**, 17723–17731.
45 G. M. Grason, B. A. DiDonna and R. D. Kamien, *Phys. Rev. Lett.*, 2003, **91**, 058304.
46 G. M. Grason, *Phys. Rep.*, 2006, **433**, 1–64.
47 K. Momma and F. Izumi, *J. Appl. Crystallogr.*, 2011, **44**, 1272–1276.
48 M. De Graef and M. McHenry, *Structure of Materials: An Introduction to Crystallography, Diffraction and Symmetry*, Cambridge University Press, 2nd edn, 2012.
49 F. Stein, M. Palm and G. Sauthoff, *Intermetallics*, 2004, **12**, 713–720.
50 K. M. Hong and J. Noolandi, *Macromolecules*, 1981, **14**, 727–736.
51 M. W. Matsen, *Phys. Rev. Lett.*, 1995, **74**, 4225–4228.
52 A. Arora, J. Qin, D. C. Morse, K. T. Delaney, G. H. Fredrickson, F. S. Bates and K. D. Dorfman, *Macromolecules*, 2016, **49**, 4675–4690.
53 M. W. Schulze, R. M. Lewis, J. H. Lettow, R. J. Hickey, T. M. Gillard, M. A. Hillmyer and F. S. Bates, *Phys. Rev. Lett.*, 2017, **118**, 1–5.
54 S. T. Milner, *Macromolecules*, 1994, **27**, 2333–2335.
55 F. S. Bates and G. H. Fredrickson, *Macromolecules*, 1994, **27**, 1065–1067.
56 A. Arora, D. C. Morse, F. S. Bates and K. D. Dorfman, *J. Chem. Phys.*, 2017, **146**, 244902.
57 R. B. Thompson, K. Ø. Rasmussen and T. Lookman, *J. Chem. Phys.*, 2004, **120**, 31–34.
58 M. W. Matsen, *Eur. Phys. J. E*, 2009, **30**, 361–369.
59 F. Stein, M. Palm and G. Sauthoff, *Intermetallics*, 2005, **13**, 1056–1074.